

Research Paper

**Modeling of Acoustic Coupling of Ultrasonic Probes
for High-Speed Rail Track Inspection**

Sławomir MACKIEWICZ, Zbigniew RANACHOWSKI*, Tomasz KATZ,
Tomasz DEBOWSKI, Grzegorz STARZYŃSKI, Przemysław RANACHOWSKI

*Institute of Fundamental Technological Research
Polish Academy of Sciences
Warsaw, Poland*

*Corresponding Author e-mail: zranach@ippt.pan.pl

(received July 5, 2023; accepted January 4, 2024; published online March 28, 2024)

The paper presents the modeling of transmission of the ultrasonic plane wave through an uniform liquid layer. The considered sources of the ultrasonic wave were normal (straight) beam longitudinal wave probes and angle beam shear waves probes commonly used in non-destructive testing. Coupling losses (CL) introduced by the presence of the coupling layer are discussed and determined applying the numerical procedure. The modeling applies to both monochromatic waves and short ultrasonic pulses with a specified frequency bandwidth. Model implementation and validation was performed using a specialized software. The predictions of the model were confirmed by coupling losses measurements for a normal beam longitudinal wave probe with a delay line made of polymethyl methacrylate (PMMA). The developed model can be useful in designing ultrasonic probes for high-speed rail track inspections, especially for establishing the optimal thickness of the water coupling layer and estimation of coupling losses, due to inevitable changes of the water gap during mobile rail inspection.

Keywords: non-destructive testing; ultrasonic examination; plane wave propagation.



Copyright © 2024 The Author(s).
This work is licensed under the Creative Commons Attribution 4.0 International CC BY 4.0
(<https://creativecommons.org/licenses/by/4.0/>).

1. Introduction

Rail track failures create a significant problem enforcing the railroad administration to permanent control of the integrity of exploited infrastructure. Both International Union of Railways [UIC] as well as Federal Railroad Administration in USA issue the legislative rules for regulating the safety of the subject railroad system (UIC, 2022; Federal Railroad Administration, 2015). A detailed codes of appropriate procedures of rail track testing can be found in European Union Standards (EN 16729-3, 2018; EN 17397-1, 2021). A remarkable challenge related to the testing procedure is the total length of the railway network, which is by UIC estimated at 260 000 kilometers.

Railway rails are exposed to high mechanical loads and challenging environmental conditions such as rolling contact fatigue, thermal stresses and corrosive environment. Due to such operational conditions different types of defects can develop in the rail head,

web, and foot (BRAY, 2000). The rolling contact defects, like wear, stripping, crushing, and fatigue cracks are distributed mainly on the surface and in the upper part of the rail head. Many of these defects can steadily grow and finally cause rail breakage, leading to derailments or more catastrophic events. Such extreme consequences can be avoided, provided that proper inspection procedures are performed and all unacceptable defects are detected before they cause the catastrophic failure.

A variety of equipment is applied for ultrasonic inspection (PAPAElias *et al.*, 2008). The simplest solution is a push-trolley. In this case the operator is moving across the track with his instrumentation at a walking pace, simultaneously interpreting the test data on a flaw detector. When a suspect defect is identified, the operator stops and manually verifies the defect type and location. The most efficient solution used for ultrasonic rail inspection is the use of specialized wagons or entire inspection trains, as it was described in

(HECKEL *et al.*, 2018). The detailed investigation has revealed that the efficient operation of the SPZ1 train is possible below 80 km/h and the practical inspection speed is highly influenced by the local quality of the track. The further progress in ultrasonic testing of railway rails depends heavily on computer modeling and simulations of all aspects of the ultrasonic inspections process (HECKEL *et al.*, 2019). One of these aspects is quality and stability of acoustic coupling between the testing probe, and the rail surface. No extensive research on this specific subject has been carried to date. One of the few published works (ZULIAN, 2022) explores the effect of the coupling media type and surface roughness on contact transfer losses. Unfortunately, in the case of automatic railway rail inspection, the only possible coupling agent is water, and the main reason for the fluctuation of transfer losses is the instability of the water layer thickness rather than roughness of the rail surface.

The inspection probes are mounted in specially designed probe holders enabling the fixed position of the probes over the tested rail. The holders are equipped with water bleeders, that provide acoustic coupling between the ultrasonic probes and the rail surface.

The quality of the acoustic coupling between the probe and the tested rail is one of the key issues, related to the high speed ultrasonic inspection of railway tracks. Under real test conditions – the gap between the rail surface and testing probes may vary due to waviness and dents on the rail surface. To ensure the continuous transmission of ultrasonic waves to the rail body, the gap must be constantly filled with water without any air bubbles or cavitation. To fulfill this critical condition, the water coupling system for high speed scanning must be designed in much greater detail than for ordinary ultrasonic inspections, where the water gap is usually undefined and uncontrolled. An example of such an ordinary probe holder, used in moderate speed inspection wagons (i.e., 30–40 km/h) is presented in Fig. 1. In such a solution – both the lower surface of the probe holder and the surfaces of ultrasonic probe wedges are pressed directly to the wetted rail surface, without any distance. It means that the water supplied by the dispensers located at the be-

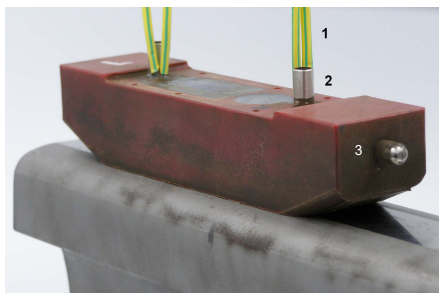


Fig. 1. General view of ultrasonic probe holder used for inspection in Polish Railways: 1 – signal cable; 2 – water coupling bleeder connector; 3 – positioning bracket.

ginning of the probe holder, can be wiped off the rail surface before it fills the gap between the active surface of the probe and the rail. Such a method has turned out to be impractical in the case of high speed rail inspection systems. In that case, other solution prefer train probe holders equipped with some abrasion resistive slides – to set the gap between the probe surface and rail surface to 0.2 mm (HECKEL *et al.*, 2009). Such an arrangement ensures better water coupling and enhances the probe lifespan.

The objective of the presented paper is to analyze in detail the influence of the probe – rail gap filled with water on the transfer losses of ultrasonic energy emitted and received by ultrasonic transducers. The practical purpose of these research is to establish optimal thickness of the water coupling layers for ultrasonic probes of different types (angle probes, normal probes), operating at different frequencies and refraction angles. It is expected that the optimal gap thickness heavily depends on ultrasonic waves frequency as well, as on the angle of incidence on wedge – rail contact. The analysis should consider not only the absolute minimization of the transfer losses but, also the minimization of ultrasonic signal fluctuation, due to inevitable variability of the water gap thickness under practical conditions. Minimization of signal fluctuations due to coupling variations is particularly important to maintain the constant sensitivity of ultrasonic inspection along the whole rail length.

In order to achieve the intended goals, the new theoretical model for calculation of transmission losses through the coupling layer was developed. The model is more general and comprehensive than simplified traditional solutions, used up to now in ultrasonic non-destructive testing and described in (KRAUTKRÄMER, KRAUTKRÄMER, 1990; OBRAZ, 1983). The first novelty is going beyond the case of perpendicular incidence of the wave on the coupling layer. Due to this, the model is applicable not only to normal beam longitudinal wave probes, but also to angle beam shear wave probes, which are commonly used in non-destructive testing. The second novelty is going beyond the case of monochromatic wave, and taking into consideration the wideband nature of modern ultrasonic probes.

The developed model was implemented in the computer program and used for example calculations, showing its compatibility with existed analytical formulas for normal incidence on the coupling layer. A very good agreement was also achieved with experimental results obtained for the typical ultrasonic probes used in non-destructive testing of railway rails.

2. Theoretical model

2.1. General considerations

In this section the general theoretical model of transmission of ultrasonic plane wave through the uni-

form liquid layer is developed. It is more general, than widely known formulas presented in ultrasonic textbooks (KRAUTKRÄMER, KRAUTKRÄMER, 1990), which consider only the normal incidence of ultrasonic wave on the contact layer. It assumes the longitudinal wave incidence at an arbitrary angle, as it actually takes place in angle beam ultrasonic probes. The theoretical treatment follows the one used by FOLDS and LOGGINS (1977) in their paper on transmission and reflection of ultrasonic waves in layered media. Compared to the mentioned theoretical work there is one important change. Folds and Loggins considered transmission of plane wave from one semi-infinite liquid media to another semi-infinite liquid media, through a system of plane-parallel solid layers. In this work, transmission of the longitudinal (L -type) wave from one semi-infinite solid media to another semi-infinite solid media through a plane parallel liquid layer, is considered. Due to this change it is possible to model, not only direct transmission of longitudinal wave, but also the transmission with transformation from a longitudinal to a transversal wave – as it actually takes place in shear wave angle beam probes, widely used in ultrasonic testing of railway rails.

The transmission of ultrasonic waves through the system of plane-parallel layers was extensively investigated, in the context of underwater sound applications for optimization of sonar domes, underwater transducer windows and reflectors. One of the first theoretical works which considered the transmission of ultrasonic plane wave through the system of plane-parallel layers at oblique incidence was by BREKHOVSKIKH (1980). As there were some restrictions concerning the validity of equations presented in that paper, the other authors (BARNARD *et al.*, 1975;

FOLDS, LOGGINS, 1977) improved the solution to be valid for a system of solid layers with arbitrary parameters. However, in all these treatments, it was assumed that both the initial and final medium is liquid – as it was natural for underwater applications.

In the case of ultrasonic angle beam probes, used for nondestructive testing, the ultrasonic wave is transmitted from a solid wedge made of PMMA or Rexolite to a solid rail material (steel), through the liquid coupling layer (water). Therefore, the considered problem is somewhat different from the mentioned hydroacoustic problems. The general scheme of a wave propagation in a coupling layer problem is shown in Fig. 2.

In the probe wedge (medium 3) there is one incident longitudinal (L -type), a wave with an arbitrary incidence angle θ_3 and two reflected waves, L -type and transversal (T -type), with reflection angles, respectively – θ_3 and θ'_3 , given by the Snell law. In the coupling layer (medium 2) there is only one refracted L -type wave and one reflected L -type wave, both with angles θ_2 to the normal. In the tested material (medium 1), there is generally one refracted L -type wave and one refracted T -type wave, with refraction angles, respectively, θ_1 and θ'_1 . But, if the incidence angle θ_3 is between the first and second critical angle there is only one, T -type wave – which propagates in medium 1. This is actually the case encountered in angle beam shear wave probes, used in nondestructive testing. However, it should be noted that instead of a sinusoidal L -type wave propagating in the tested material, there exists so called evanescent L -type wave, exponentially decaying from the material surface as in the work (SCHMERR JR., 2016). It must be included in the theoretical model, despite the fact that it has no practical significance.

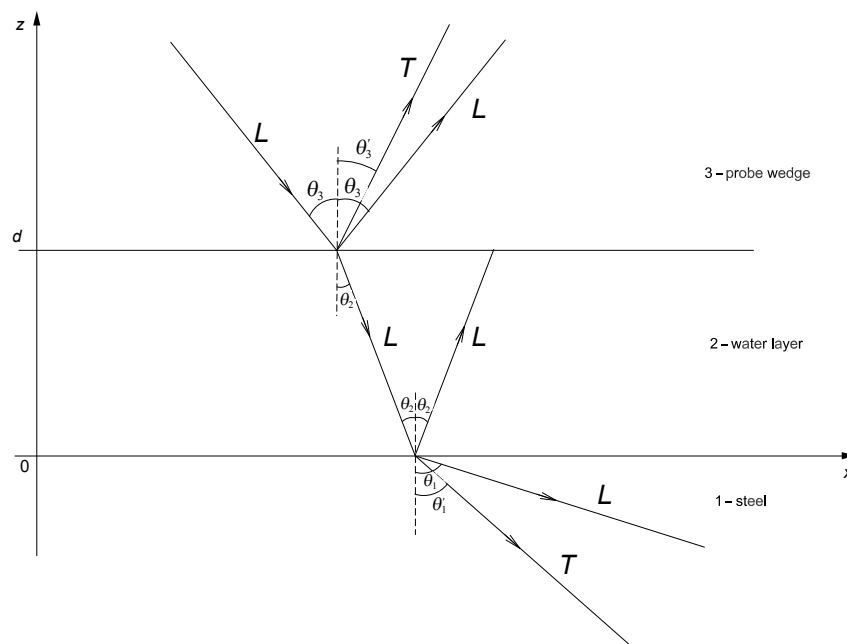


Fig. 2. General scheme of a coupling layer problem.

The all three media are assumed to be perfectly elastic and isotropic with Lamé moduli: λ_i , μ_i , mass density ρ_i , and ultrasonic velocities of longitudinal waves $C_{l_i} = \sqrt{(\lambda_i + 2\mu_i)/\rho_i}$, and transversal waves $C_{t_i} = \sqrt{\mu_i/\rho_i}$, respectively. Index i denotes the number of medium (1, 2 or 3), as indicated in Fig. 2. For harmonic waves the time dependence for all considered waves is given by a factor $\exp(i\omega t)$, which is neglected in further considerations.

The problem is solved using potential functions for the particle velocity φ_i – for longitudinal waves and ψ_i – for transversal waves. The Cartesian coordinate z is normal to the coupling layer, the coordinate x lies in the plane of incidence, and the coordinate y is normal to the plane of incidence. For the geometrical configuration shown in Fig. 2 the explicit forms of potential functions in media 1, 2, and 3 are:

$$\begin{aligned} & \text{– in medium 1:} \\ & \varphi_1 = B_1 e^{-i(\alpha_1 z - \sigma x)}, \\ & \psi_1 = D_1 e^{-i(\beta_1 z - \sigma x)}, \end{aligned} \quad (1)$$

$$\begin{aligned} & \text{– in medium 2:} \\ & \varphi_2 = B_2 e^{-i(\alpha_2 z - \sigma x)} + A_2 e^{i(\alpha_2 z - \sigma x)}, \\ & \psi_2 = 0; \end{aligned} \quad (2)$$

$$\begin{aligned} & \text{– in medium 3:} \\ & \varphi_3 = B_3 e^{-i(\alpha_3 z - \sigma x)} + A_3 e^{i(\alpha_3 z - \sigma x)}, \\ & \psi_3 = C_3 e^{i(\beta_3 z + \sigma x)}, \end{aligned} \quad (3)$$

where α_i are the z -coordinates of wave vectors of the longitudinal wave, β_i are the z -coordinates of the wave vectors of the transversal waves, A_i are the amplitudes of potential functions for L -type waves traveling in the positive z -direction, B_i are the amplitudes of potential functions for L -type waves traveling in the negative z -direction, C_i are the amplitudes of potential functions for T -type waves traveling in the positive z -direction, and D_i are the amplitudes of potential functions for T -type waves traveling in the negative z -direction.

The σ symbol indicates the x -coordinate of all the wave vectors. They have to be equal to meet the continuity conditions at the interfaces. Actually, this is a condition equivalent to the Snell law, and can be expressed as:

$$\begin{aligned} \sigma &= k_{l1} \sin \theta_1 = k_{t1} \sin \theta'_1 = k_{l2} \sin \theta_2 \\ &= k_{l3} \sin \theta_3 = k_{t3} \sin \theta'_3, \end{aligned} \quad (4)$$

where $k_{li} = \frac{\omega}{C_{li}}$ is the wave number of longitudinal wave in the i -th medium and $k_{ti} = \frac{\omega}{C_{ti}}$ is the wave number of transversal wave in the i -th medium.

Consequently, the z -coordinates of the wave vectors in the three media are given by the formulas:

$$\begin{aligned} & \text{– in medium 1:} \\ & \alpha_1 = \sqrt{k_{t1}^2 - \sigma^2}, \quad \beta_1 = \sqrt{k_{t1}^2 - \sigma^2}; \end{aligned} \quad (5)$$

$$\begin{aligned} & \text{– in medium 2:} \\ & \alpha_2 = \sqrt{k_{t2}^2 - \sigma^2}; \end{aligned} \quad (6)$$

$$\begin{aligned} & \text{– in medium 3:} \\ & \alpha_3 = \sqrt{k_{t3}^2 - \sigma^2}, \quad \beta_3 = \sqrt{k_{t3}^2 - \sigma^2}. \end{aligned} \quad (7)$$

It should be noted that z -coordinate of wave vector of longitudinal wave in medium 1 (tested material) can be a real value – for incidence angles below the 1st critical angle or an imaginary value – for incidence angles above the 1st critical angle. The z -coordinates of all other wave vectors are real, as we consider only practical cases, where the incidence angle is below the 2nd critical angle.

The particle velocities and stresses of all considered waves can be determined from potential functions by the following formula. For simplicity we neglect the media indexes i , since the form of these formulas is the same for all media:

$$v_x(z) = \frac{\partial \varphi}{\partial x} - \frac{\partial \psi}{\partial z}, \quad (8)$$

$$v_z(z) = \frac{\partial \varphi}{\partial z} + \frac{\partial \psi}{\partial x}, \quad (9)$$

$$T_{zz}(z) = \frac{i}{\omega} \left(\lambda \frac{\partial v_x}{\partial x} + \lambda \frac{\partial v_z}{\partial z} + 2\mu \frac{\partial v_z}{\partial z} \right), \quad (10)$$

$$T_{xz}(z) = \frac{i}{\omega} \left(\mu \frac{\partial v_x}{\partial z} + \mu \frac{\partial v_z}{\partial x} \right). \quad (11)$$

Substituting into these formulas potential functions given by Eqs. (1), (2), (3) and doing some ordering, the particle velocities and stresses in each medium can be expressed as the linear combinations of the amplitudes of relevant potential functions.

In medium 1:

$$v_x^1(z) = i\sigma e^{-i\alpha_1 z} e^{i\sigma x} B_1 + i\beta_1 e^{-i\beta_1 z} e^{i\sigma x} D_1, \quad (12)$$

$$v_z^{(1)}(z) = -i\alpha_1 e^{-i\alpha_1 z} e^{i\sigma x} B_1 + i\sigma e^{-i\beta_1 z} e^{i\sigma x} D_1, \quad (13)$$

$$T_{zz}^{(1)}(z) = -ie_1 e^{-i\alpha_1 z} e^{i\sigma x} B_1 + ig_1 \beta_1 e^{-i\beta_1 z} e^{i\sigma x} D_1, \quad (14)$$

$$T_{xz}^{(1)}(z) = ig_1 \alpha_1 e^{-i\alpha_1 z} e^{i\sigma x} B_1 + ie_1 e^{-i\beta_1 z} e^{i\sigma x} D_1, \quad (15)$$

where $e_1 = (\lambda_1 k_{l1}^2 + 2\mu_1 \alpha_1^2) / \omega$ and $g_1 = 2\mu_1 \sigma / \omega$.

In medium 2:

$$v_x^{(2)}(z) = i\sigma e^{i\alpha_2 z} e^{i\sigma x} A_2 + i\sigma e^{-i\alpha_2 z} e^{i\sigma x} B_2, \quad (16)$$

$$v_z^{(2)}(z) = i\alpha_2 e^{i\alpha_2 z} e^{i\sigma x} A_2 - i\alpha_2 e^{-i\alpha_2 z} e^{i\sigma x} B_2, \quad (17)$$

$$T_{zz}^{(2)}(z) = -ie_2 e^{i\alpha_2 z} e^{i\sigma x} A_2 - ie_2 e^{-i\alpha_2 z} e^{i\sigma x} B_2, \quad (18)$$

$$T_{xz}^{(2)}(z) = 0, \quad (19)$$

where $e_2 = \lambda_2 k_{l2}^2 / \omega$ and $T_{xz}^{(1)}(z) = 0$ because medium 2 is a liquid and does not transfer shear stresses.

In medium 3:

$$v_x^{(3)}(z) = i\sigma e^{i\alpha_3 z} e^{i\sigma x} A_3 + i\sigma e^{-i\alpha_3 z} e^{i\sigma x} B_3 - i\beta_3 e^{i\beta_3 z} e^{i\sigma x} C_3, \quad (20)$$

$$v_z^{(3)}(z) = i\alpha_3 e^{i\alpha_3 z} e^{i\sigma x} A_3 - i\alpha_3 e^{-i\alpha_3 z} e^{i\sigma x} B_3 + i\sigma e^{i\beta_3 z} e^{i\sigma x} C_3, \quad (21)$$

$$T_{zz}^{(3)}(z) = -ie_3 e^{i\alpha_3 z} e^{i\sigma x} A_3 - ie_3 e^{-i\alpha_3 z} e^{i\sigma x} B_3 - ig_3 \beta_3 e^{i\beta_3 z} e^{i\sigma x} C_3, \quad (22)$$

$$T_{xz}^{(3)}(z) = -ig_3 \alpha_3 e^{i\alpha_3 z} e^{i\sigma x} A_3 + ig_3 \alpha_3 e^{-i\alpha_3 z} e^{i\sigma x} B_3 + ie_3 e^{i\beta_3 z} e^{i\sigma x} C_3, \quad (23)$$

where $e_3 = (\lambda_3 k_{l3}^2 + 2\mu_3 \alpha_3^2) / \omega$ and $g_3 = \frac{2\mu_3 \sigma}{\omega}$.

Now, we consider the boundary conditions for particle velocities and stresses at the borders $z = 0$ and $z = d$. Both borders are between solid and liquid medium and we neglect viscosity of the liquid medium – in our case water. It follows that there is no continuity of tangential displacements and particle velocities at the borders. Consequently the boundary conditions are:

– at the border $z = 0$:

continuity of normal particle velocities

$$v_z^{(1)}(0) = v_z^{(2)}(0), \quad (24)$$

continuity of normal stresses

$$T_{zz}^{(1)}(0) = T_{zz}^{(2)}(0), \quad (25)$$

zeroing of tangential stresses in the solid media

$$T_{xz}^{(1)}(0) = 0; \quad (26)$$

– at the border $z = d$:

continuity of normal particle velocities

$$v_z^{(3)}(d) = v_z^{(2)}(d), \quad (27)$$

continuity of normal stresses

$$T_{zz}^{(3)}(d) = T_{zz}^{(2)}(d), \quad (28)$$

zeroing of tangential stresses in the solid media

$$T_{xz}^{(3)}(d) = 0. \quad (29)$$

Substituting Eqs. (12)–(23) to the above boundary conditions there are obtained six complex equations, for six unknown amplitudes of potential functions: A_3 , C_3 , A_2 , B_2 , B_1 , D_1 . The amplitude B_3 is the amplitude

of incident longitudinal wave, so it is a known value which can be set to 1.

The obtained set of six linear equations can be conveniently expressed in a matrix form to facilitate further numerical processing:

$$\begin{bmatrix} \alpha_3 e^{i\alpha_3 d} & \sigma e^{i\beta_3 d} & -\alpha_2 e^{i\alpha_2 d} & \alpha_2 e^{-i\alpha_2 d} & 0 & 0 \\ -e_3 e^{i\alpha_3 d} & -g_3 \beta_3 e^{i\beta_3 d} & e_2 e^{i\alpha_2 d} & e_2 e^{-i\alpha_2 d} & 0 & 0 \\ -g_3 \alpha_3 e^{i\alpha_3 d} & e_3 e^{i\beta_3 d} & 0 & 0 & 0 & 0 \\ 0 & 0 & \alpha_2 & -\alpha_2 & \alpha_1 & -\sigma \\ 0 & 0 & -e_2 & -e_2 & e_1 & -g_1 \beta_1 \\ 0 & 0 & 0 & 0 & g_1 \alpha_1 & e_1 \end{bmatrix} \begin{bmatrix} A_3 \\ C_3 \\ A_2 \\ B_2 \\ B_1 \\ D_1 \end{bmatrix} = \begin{bmatrix} \alpha_3 e^{-i\alpha_3 d} \\ e_3 e^{-i\alpha_3 d} \\ -g_3 \alpha_3 e^{-i\alpha_3 d} \\ 0 \\ 0 \\ 0 \end{bmatrix}, \quad (30)$$

or

$$[M] [X] = [Y]. \quad (31)$$

By inverting this matrix equation, all unknown A_3 , C_3 , A_2 , B_2 , B_1 , D_1 amplitudes of potential functions in media 1, 2 and 3 are obtained:

$$[X] = [M]^{-1} [Y], \quad (32)$$

or

$$\begin{bmatrix} A_3 \\ C_3 \\ A_2 \\ B_2 \\ B_1 \\ D_1 \end{bmatrix} = [M]^{-1} \begin{bmatrix} \alpha_3 e^{-i\alpha_3 d} \\ e_3 e^{-i\alpha_3 d} \\ -g_3 \alpha_3 e^{-i\alpha_3 d} \\ 0 \\ 0 \\ 0 \end{bmatrix}. \quad (33)$$

In this work the main subject of interest is the transmission coefficient of the ultrasonic wave from medium 3 (probe wedge) to medium 1 (tested material). For the standard angle beam shear wave probes, i.e., for cases when the incident angle is between the 1st and the 2nd critical angle, this coefficient is given by:

$$T_{3-1}^{L-T} = \frac{D_1}{B_3} = \frac{D_1}{1} = D_1. \quad (34)$$

For angle beam longitudinal wave probes, i.e., for cases where the incident angle is below the 1-st critical angle, this coefficient is given by:

$$T_{3-1}^{L-L} = \frac{B_1}{B_3} = \frac{B_1}{1} = B_1. \quad (35)$$

In non-destructive testing procedures, the ultrasonic pulse passes through the coupling layer twice, first

when it is introduced to the tested material, and second – on its way back, after reflection from the defect. So, from practical point of view, the most interesting is the double transmission coefficient, i.e., the product of transmission coefficients from medium 3 to 1 and from medium 1 to 3.

For shear wave probes it is given by:

$$T_{3-1-3}^{L-T-L} = T_{3-1}^{L-T} \cdot T_{1-3}^{T-L}. \quad (36)$$

For longitudinal wave probes it is given by:

$$T_{3-1-3}^{L-L-L} = T_{3-1}^{L-L} \cdot T_{1-3}^{L-L}. \quad (37)$$

The inverse transmission coefficients T_{1-3}^{T-L} and T_{1-3}^{L-L} could be determined from properly redefined models similar to the one given in Fig. 2. However, most easily they can be calculated from the direct transmission coefficients using the so-called Stokes' relations (SCHMERR JR., 2016). Applying these relations we obtain, respectively:

$$T_{1-3}^{T-L} = T_{3-1}^{L-T} \cdot \frac{Cl_1 \rho_1 \cos \theta'_1}{Cl_3 \rho_3 \cos \theta_3} \quad (38)$$

and

$$T_{1-3}^{L-L} = T_{3-1}^{L-L} \cdot \frac{Cl_1 \rho_1 \cos \theta_1}{Cl_3 \rho_3 \cos \theta_3}. \quad (39)$$

Finally, substituting (38) and (39) to (36) and (37), the sought formulas for double transmission coefficients, for both types of ultrasonic probes used in non-destructive testing are obtained. The formulas take into account the liquid coupling layer of thickness d , between the probe wedge and tested material:

$$\begin{aligned} T_{3-1-3}^{L-T-L} &= (T_{3-1}^{L-T})^2 \cdot \frac{Cl_1 \rho_1 \cos \theta'_1}{Cl_3 \rho_3 \cos \theta_3} \\ &= D_1^2 \frac{Cl_1 \rho_1 \cos \theta'_1}{Cl_3 \rho_3 \cos \theta_3} \end{aligned} \quad (40)$$

and

$$\begin{aligned} T_{3-1-3}^{L-L-L} &= (T_{3-1}^{L-L})^2 \cdot \frac{Cl_1 \rho_1 \cos \theta_1}{Cl_3 \rho_3 \cos \theta_3} \\ &= B_1^2 \frac{Cl_1 \rho_1 \cos \theta_1}{Cl_3 \rho_3 \cos \theta_3}. \end{aligned} \quad (41)$$

The aforementioned formulas, for double transmission coefficients, are derived for harmonic plane waves with a strictly defined frequency. In practice, the ultrasonic pulses generated by ultrasonic probes have a specified frequency spectrum, characterized by the so-called relative bandwidth parameter defined as:

$$\text{WB} = \frac{f_u - f_l}{f_0} \cdot 100\%, \quad (42)$$

where f_u – upper frequency of the –6 dB frequency spectrum, f_l – lower frequency of the –6 dB frequency spectrum, $f_0 = \frac{f_u + f_l}{2}$ – center frequency of the –6 dB frequency spectrum.

It means that the actual drop of amplitude of an ultrasonic pulse, traveling through the coupling layer from the probe to the tested material and vice versa, is a certain average of the double transmission coefficients for all frequencies represented in the pulse spectrum. To include this effect in the discussed model, a certain frequency spectrum is assumed for ultrasonic pulse incident on the boundary between the probe wedge and the coupling layer. Such an initial spectrum distribution can be reasonably approximated by the Gaussian function, given by:

$$G_i(f) = \exp\left(-\frac{(f - f_0)^2}{2\sigma^2}\right), \quad (43)$$

where f_0 is the center frequency of the ultrasonic probe. The parameter $\sigma = \text{WB}/235$ is defined so that the modeled spectrum has a bandwidth equal to the actual bandwidth parameter WB of the ultrasonic probe. The WB parameter is usually presented in the probe certificate or can be measured according to EN ISO 22232-2 (2020).

The signal waveform of the initial pulse in the time domain is given by the inverse Fourier transform of its spectrum:

$$h_i(t) = \int_{-\infty}^{\infty} G_i(f) e^{i2\pi ft} df. \quad (44)$$

After the double passage of the ultrasonic pulse through the coupling layer its spectrum is modified by the double transmission coefficient in the following way:

$$G_t(f) = G_i(f) \cdot T_{3-1-3}^{L-T-L}(f) \quad (45)_1$$

for the shear wave probes, and

$$G_t(f) = G_i(f) \cdot T_{3-1-3}^{L-L-L}(f) \quad (45)_2$$

for the longitudinal wave probes.

Knowing the spectrum of the double transmitted ultrasonic pulse, its signal waveform may be calculated using the inverse Fourier transform:

$$h_t(t) = \int_{-\infty}^{\infty} G_t(f) e^{i2\pi ft} df. \quad (46)$$

Then, the double transmission coefficient for the ultrasonic pulse in a time domain may be calculated according to the formula:

$$T_{3-1-3}^{L-T(L)-L}(f_0, \text{WB}) = \frac{\max\{|h_t(t)|\}}{\max\{|h_i(t)|\}}. \quad (47)$$

The designation $T^{T(L)}$ denotes here that the formula is valid for T^{L-T-L} , and for T^{L-L-L} configurations. The above definition of the double transmission coefficient in the time domain, corresponds to the experimental measurements of this value, where one compares the maximum amplitudes of the ultrasonic pulse

before and after double passage through the coupling layer. The arguments f_0 and WB, specified to the double transmission coefficient in the time domain, indicate that its value depends not only on the central frequency of the ultrasonic probe (as it is the case in the monochromatic model), but also on the probe bandwidth defined by its WB parameter.

2.2. Model implementation and validation

The described theoretical model was implemented in the prepared computer program TransmissionLoss 1.x of which the main purpose was to facilitate the design of ultrasonic probes for the new, high speed inspection wagon for the Polish Railways. In contrast to the known analytical solutions, the program allowed for calculation of double transmission coefficients and related transfer losses. It was possible not only for normal beam longitudinal wave probes, but also for angle beam shear wave probes and angle beam longitudinal wave probes, which are used in ultrasonic testing of railway rails. Moreover, the program took into account the finite bandwidth of modern ultrasonic probes, what considerably changes the dependence of transfer losses on the coupling layer thickness.

To use effectively the formulas quoted in Sec. 2 in the computer program they have to be discretized. In particular, the continuous initial pulse spectrum defined by Eq. (43) was replaced by a discretized spectrum given by dependency:

$$G_i(n\Delta f) = \exp\left(-\frac{\left(\frac{n-32}{32}\right)^2}{2\sigma^2}\right), \quad (48)$$

where $\Delta f = f_0/32$ was specified as a step in the frequency domain and integer n was changing from 1 to 63, to embrace frequency spectrum from $\frac{1}{32}f_0$ to near $2f_0$. The bandwidth of majority of ultrasonic probes, used in non-destructive testing, lies between 30% and 80% of f_0 , so their -6 dB spectrum is within the range from $0.6f_0$ to $1.4f_0$. It means that the assumed discretization range is sufficient for that application.

After calculation of the discretized initial spectrum, the program numerically inverted the matrix Eq. (30) for every discrete frequency $n\Delta f$ – within the probe spectrum – and calculates complex amplitudes $D_1(n\Delta f)$ and $B_1(n\Delta f)$. Based on these amplitudes, the double transmission coefficients $T_{3-1-3}^{L-T-L}(n\Delta f)$ and $T_{3-1-3}^{L-L-L}(n\Delta f)$ were calculated from Eqs. (40) and (41), for every discrete frequency in the probe spectrum.

Then the discrete inverse Fourier transforms were calculated for the initial pulse spectrum $G_i(n\Delta f)$ and for the pulse spectrum after double transmission through the coupling layer $G_t(n\Delta f) = T_{3-1-3}^{L-T-L}(n\Delta f)G_i(n\Delta f)$ using the FFT algorithm for

$N = 1024$ point. As a result, discrete time waveforms for initial pulse $h_i(k\Delta t)$ and after transmission pulse $h_t(k\Delta t)$ were obtained, where Δt is the time step in the time domain, and k is integer from 0 to N . The time domain step Δt is related to the Δf step and the number of points in the FFT transform by relation:

$$\Delta t = \frac{1}{N \cdot \Delta f} = \frac{1}{1024 \cdot \Delta f}. \quad (49)$$

For example, for a typical ultrasonic probe with central frequency $f_0 = 2$ MHz and time period $T_0 = 0.5 \mu s$ the frequency domain step $\Delta f = f_0/32 = 0.0625$ MHz, and the time domain step $\Delta t = 0.015625 \mu s = 1/32T_0$. It means that the discretization of waveform functions $h_i(t)$ and $h_t(t)$ can produce quantization error not greater than 0.5%, when estimating maxima of these functions from its discrete representations in Eq. (47). In non-destructive testing 0.5% error in evaluation of the ultrasonic signal amplitude is negligible – so the implemented calculation algorithm is sufficient for the intended application. On the other hand, it is fast enough to be executed on a typical personal computer.

In ultrasonic testing practice signal amplitudes relations were commonly expressed using a logarithmic scale, so the signal amplitude drop, caused by its double transmission through the coupling layer, can be conveniently expressed in decibels by the transfer losses (TL) defined as:

$$TL = -20 \log_{10} \left(T_{3-1-3}^{L-T(L)-L} \right). \quad (50)$$

The TL defined in Eq. (50) include the signal amplitude drops caused not only by the presence of the coupling layer, but also by the impedance mismatch between the material of ultrasonic probe wedge and the material tested. In many practical applications, such as ultrasonic testing of railway rails, the impedance mismatch is the same throughout the entire inspection process, and the only changing factor is the thickness of the coupling layer between the probe and the tested material. To focus attention on this dependency a more suitable parameter called coupling losses CL can be defined:

$$CL(d) = TL(d) - TL(0), \quad (51)$$

where d is the thickness of the coupling layer and $TL(0)$ are the transfer losses, calculated for the thickness d set to 0.

Due to such a definition, the coupling losses were zero for the best case scenario (the zero coupling layer) and allow for analyzing changes in the transfer losses, due to fluctuations of the coupling layer thickness. This is an important aspect of every mechanized ultrasonic inspection, as the changes in the transfer losses – due to fluctuations of the coupling layer thickness – cause uncontrolled changes in testing sensitivity during ultrasonic scanning. Knowing the characteristic of sensitivity changes as a function of coupling layer thickness, some scanning gain corrections can be applied to

compensate for the predicted sensitivity drops. This way, the coupling layer thickness fluctuations during actual examination can only increase testing sensitivity, which is a more secure situation than uncontrolled sensitivity drops.

The developed model was checked against the known analytic solution for monochromatic longitudinal plane wave incident on the coupling layer at an incident angle $\theta_3 = 0^\circ$ (see Fig. 2). The analytic formula for the transmission coefficient through the layer was taken from work (OBRAZ, 1983) and rewritten using the notations defined in this work:

$$T_{3-1}^{L-L} = 2 \left[\left(1 + \frac{\rho_3 Cl_3}{\rho_1 Cl_1} \right)^2 \left(\cos \frac{2\pi df}{Cl_2} \right)^2 + \left(\frac{\rho_2 Cl_2}{\rho_1 Cl_1} + \frac{\rho_3 Cl_3}{\rho_2 Cl_2} \right)^2 \left(\sin \frac{2\pi df}{Cl_2} \right)^2 \right]^{-\frac{1}{2}}. \quad (52)$$

The reverse transmission coefficient T_{1-3}^{L-L} can be calculated from Eq. (52) by interchanging indexes 1 and 3. Then the double transmission coefficient from medium 3 to 1 and back can be calculated as $T_{3-1}^{L-L} \cdot T_{1-3}^{L-L}$ in the same way as in Eq. (37) of the model developed in this work.

The example calculations executed using the above analytic formula and our more general numerical model, in which we assumed the monochromatic wave and incident angle $\theta_3 = 0^\circ$, were shown in Table 1. The calculations were performed for typical conditions encountered in a railway rail inspection – i.e., for 2 MHz L -type probe with the PMM wedge and assuming water coupling layer changes from 0.0 to 0.5 mm.

Table 1. Comparison of coefficient T_{3-1-3}^{L-L-L} , calculated for 2 MHz longitudinal monochromatic wave and incident angle $\theta_3 = 0^\circ$, applying the proposed model (Eq. (41)) and by the analytic Eq. (52).

d [mm]	T_{3-1-3}^{L-L-L}	
	model	analytic formula
0.00	0.242355	0.242355
0.05	0.156465	0.156465
0.10	0.085844	0.085844
0.15	0.061231	0.061231
0.20	0.057934	0.057934
0.25	0.072430	0.072430
0.30	0.120302	0.120302
0.35	0.221854	0.221854
0.40	0.201053	0.201053
0.45	0.106440	0.106440
0.50	0.067703	0.067703

The aforementioned calculations were performed using double precision arithmetic. As can be seen from Table 1, the results of the presented numerical model and the known analytic solution match up to six decimal places. It could be expected, as both approaches

assume the same problem geometry and boundary conditions. It is a prove however, that the rather complicated model implementation, based on the numerical solution of a complex 6×6 equation set, does not contain any errors in the program algorithms.

3. Experimental verification of modeling results

The preliminary experimental verification of the developed model was performed using the commercial ultrasonic probe Panametrics A106 integrated with a delay line (probe wedge) made of PMMA. The probe was of the longitudinal wave and of the straight ($\theta_3 = 0^\circ$) beam type, with the nominal frequency 2.25 MHz and the transducer diameter of 12.5 mm. The spectral characteristic of the probe with the PMMA delay line was determined using the laboratory system comprising Panametrics Epoch 650 Pulser/Receiver/Digitizer, Calibration Block No 1 (according to ISO 2400), and proprietary software implementing the Fourier transform using the FFT algorithm.

The details of the experimental setup are presented in Fig. 4. The central frequency f_0 and -6 dB bandwidth BW were determined according to EN 12668-2:2010 applying the measured transmitting-receiving spectral characteristic. The lower band frequency was $f_l = 1.17$ MHz, and the upper $f_u = 2.58$ MHz. Applying the abovementioned data, the central frequency and relative bandwidth of the probe coupled with the delay line, were calculated using the following standard formulas:

$$f_0 = \frac{(f_l + f_u)}{2} = \frac{1.17 + 2.58}{2} = 1.88 \text{ MHz}, \quad (53)$$

$$\text{BW} = \frac{2(f_u - f_l)}{(f_u + f_l)} 100\% = \frac{1.41}{1.88} 100 = 75\%. \quad (54)$$

The parameters BW and f_0 were introduced to the presented model, that takes into account the bandwidth of the probe. It was performed applying Eq. (43) to calculate CL introduced by a thin water layer placed between the delay line of the probe and the steel block representing the tested material. The conceptual scheme of this experimental setup is shown in Fig. 3.

According to this diagram, the piezoelectric transducer of the ultrasonic probe transmits to the PMMA delay line a short pulse of longitudinal wave, which travels to the coupling layer of a thickness d on the border between the delay line and the steel block. Part of the ultrasonic energy reflects on the border layer, creating on the screen of the ultrasonic receiver the first ultrasonic echo (so called interface echo with amplitude A_0), which is normally of no importance for ultrasonic testing. The other part of the ultrasonic energy passes through the coupling layer to the steel block and reflects from its bottom giving a so-called back wall echo of amplitude A_1 . The amplitude of this echo

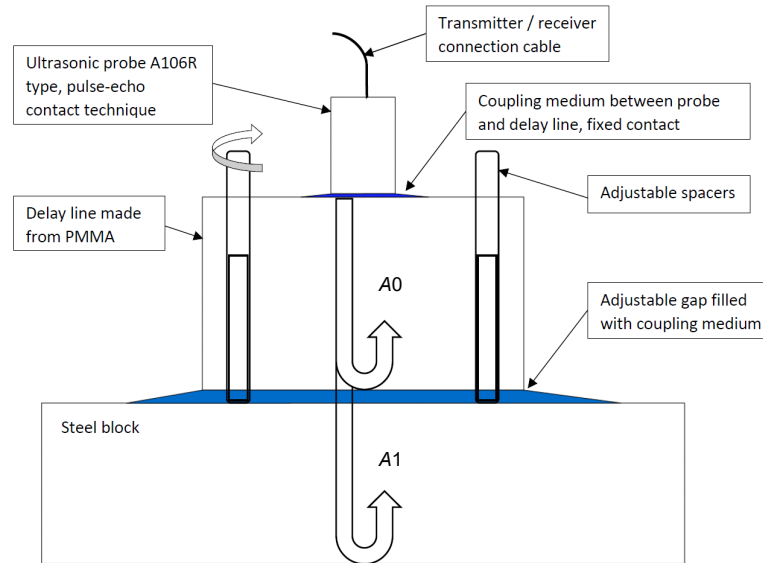


Fig. 3. Scheme of the experimental setup used for verification of theoretical models for calculation of CL, introduced by water coupling layer between PMMA delay line and the steel block (look for a description in the text).

depends on the double transmission coefficient through the coupling layer, but also on all other factors affecting the pulse on the way from the sending transducer to the bottom surface of the steel block, and after reflection on the way back to the receiving transducer:

$$A1 = A0 S_{a3} S_{d3} S_{a1} S_{d1} R_1 T_{3-1-3}^{L-L-L}, \quad (55)$$

where $A0$ – the initial amplitude of the ultrasonic pulse near the sending transducer, T_{3-1-3}^{L-L-L} – the two way transmission coefficient through the coupling layer, S_{a3} – attenuation of the signal amplitude in the PMMA delay line (medium 3), S_{d3} – diffraction divergence losses in the PMMA delay line, S_{a1} – attenuation of the signal amplitude in the steel block (medium 1), S_{d1} – diffraction divergence losses in the steel block, R_1 – reflection coefficient at the bottom surface of the steel block.

The double transmission coefficient, and in consequence the amplitude of the back wall echo $A1$, depends on the thickness of the coupling layer d . For practical applications, this dependence is most conveniently expressed in terms of CL, defined by Eqs. (51) and (50). In the presented experiment, coupling losses are determined by the ratio of back wall echo amplitudes, obtained for the coupling layer of a thickness d to the back wall echo amplitude for the coupling layer thickness equal to zero. It is expressed in decibels by the formula:

$$CL(d) = -20 \log_{10} \left(\frac{A1(d)}{A1(0)} \right). \quad (56)$$

It should be noted, that in an experimental approach described here, it can be determined the coupling losses without considering the ultrasonic attenuation and beam divergence in the PMMA delay line

and the steel block as well as considering the reflection coefficient of the ultrasonic pulse at the bottom of the steel block. All these factors obviously affect the measured amplitudes of back wall echoes but are independent of the thicknesses of the coupling layer and are reduced in the fractional expression of Eq. (56).

The photograph of the experimental setup, used for determination of CL, depending on the coupling layer thickness d , is shown in Fig. 4. The distance d between the PMMA delay line and the steel block was adjusted using three fine-pitch screws. This distance was controlled using a dial micrometer with accuracy of ± 0.001 mm. During measurements the steel block and a lower part of the delay line were immersed in

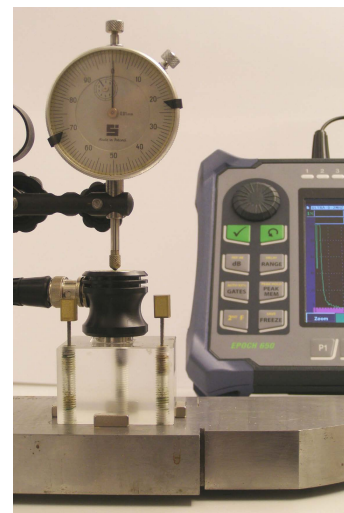


Fig. 4. Photograph of the experimental setup to determine CL, introduced by water coupling layer existing between a PMMA delay line and a steel block.

water to ensure complete filling with water of the gap between these objects.

The first step of the performed procedure was to determine the back wall echo amplitude for the coupling layer of zero thickness – $A1(0)$. During this step, the distancing screws were released and the PMMA plate was slightly pressed against the steel block to remove any remaining water between them. Within the next steps the distance between the coupled objects, representing the thickness of the water coupling layer d , was steadily increased, and back wall echo amplitudes $A1(d)$ were measured. Finally, the measured echo amplitudes were substituted to Eq. (56) and CL in dependence of d , were determined. The measurements were performed for a water layer thickness in the range from 0.0 to 0.8 mm, which embrace the coupling layer thickness fluctuations, that can be reasonably expected in actual rail testing.

The results of experimental measurements of $CL(d)$ are presented in Fig. 5 with discrete points (squares). The range of measurement errors was determined based on the spread of twelve measurements for each point. The continuous line presents a theoretical curve calculated for the considered setup using the wideband model, and the dashed line depicts the theoretical curve calculated from the basic monochromatic model. It can be seen that in an initial thickness range (up to ca. 0.15 mm), the agreement between experimental results and both theoretical curves is very good. Then the experimental results and model predictions start to diverge. The curve calculated from the monochromatic model presents much larger deviations from the experimental data than the curve calculated applying the wideband model. This is especially visible for the layer thicknesses above 0.2 mm, where the more precise model still gives reasonable approximation of experimental data, while the basic monochromatic model completely fails showing nonexistent minima and maxima of coupling losses. In general, the wideband model predicts slightly higher values of coupling losses than experimental data, however, the difference does not exceed 1.0 dB at any measurement point. This can be assessed as a quite sufficient

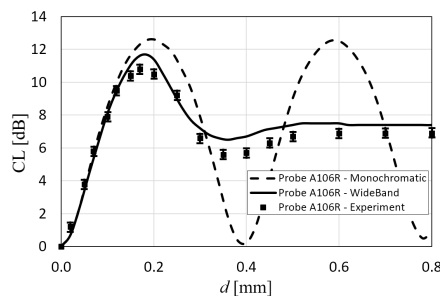


Fig. 5. Comparison of experimentally determined CL introduced by water coupling layer with theoretical calculations using the proposed wideband model and a commonly known monochromatic model.

modeling accuracy from the point of view of practical applications in automated ultrasonic examinations.

4. Exploration of model implications for railway rail testing

One of the most important factors, affecting the reliability of ultrasonic inspections of railway rails, is dependence of testing sensitivity on the random changes of coupling between scanning probes and the rail surface. Fluctuations of coupling layer thickness during high speed ultrasonic scanning are unavoidable due to waviness of the rail surface and spring suspension of ultrasonic probes.

According to widely known monochromatic Eq. (52) dependence of CL on the water layer thickness d is periodic – as shown in Fig. 6 – with a black color curve. The results were calculated for the probe of a longitudinal wave and of $\theta_3 = 0^\circ$ beam type. In this approximation the minima of the coupling losses occur periodically at $d = n \frac{\lambda_2}{2}$ that is, at multiples of half the wavelength in the coupling layer. It is rather a theoretical result not observed in the ultrasonic testing practice.

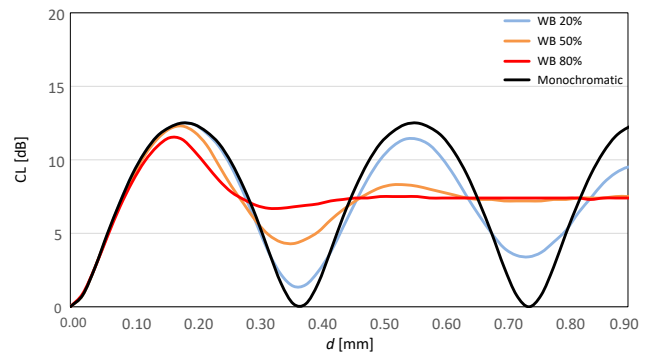


Fig. 6. Dependences of CL versus the water layer thickness, calculated for 2 MHz L -type probes, with different relative bandwidths WB.

To investigate this problem in more detail, there was calculated, applying the wideband model, coupling losses characteristics for the same 2 MHz frequency, but assuming three typical bandwidths of commercial ultrasonic probes, ranging from 20 to 80%. The calculation results are shown in Fig. 6 with colored curves. For the typical narrow band probe (WB = 20%) the characteristic is similar to the monochromatic case, but successive minima are getting shallower and coupling losses reach zero value only for the layer thickness equal to zero. For most common medium band probes (WB = 50%), there is only one additional minimum at $d = \frac{\lambda_2}{2}$ but it is much shallower than the minimum observed at the zero thickness layer. For wide band probes (WB = 80%), there is no additional minima and only one maximum of coupling losses observed at $d = \frac{\lambda_2}{4}$. After this maximum, the characteristic flattens out and shows no significant changes in coupling losses.

The presented results confirm the statement, that the bandwidth of ultrasonic probes has a significant effect on the coupling losses during ultrasonic scanning, and should be taken into account when designing and during calibration of ultrasonic inspection systems. For a typical 2 MHz *L*-type probe with medium bandwidth (parameter WB = 50%), the maximum coupling losses of 12.3 dB occur at the coupling layer thickness of 0.18 mm, and falls rapidly to zero with reduction of the layer thickness. It corresponds to 12.3 dB fluctuations in testing sensitivity between different sections of the tested rail, regarding the worst case scenario. To avoid such big changes in testing sensitivity, the minimum thickness of the coupling layer should be limited to ca. 0.1 mm, by fixing a distancing pins made of the hard material in the probe scanning surface. In this way, the fluctuations of testing sensitivity could be reduced from 12.3 to about 8 dB.

In addition to the analysis of the operation of 2 MHz *L*-type probes, it is interesting to determine how the coupling layer thickness affects the transfer losses determined for angle beam shear wave probes, commonly used in railway rail inspections.

As can be seen from Fig. 7, coupling losses characteristics are almost the same for *L*-type probe and *T*-type probes with refraction angles of 45° and 70°, assuming they have the same central frequency and bandwidth. However, if the central frequency of the probe would change, the coupling losses characteristic also change considerably, as can be seen in Fig. 8. Increase of the probe frequency from 2 to 4 MHz contracts the characteristic curve by a factor 2 on the layer thickness axis. It means that for 4 MHz probes the minimum separation between the probe faces and the rail surface could be reduced to 0.05 mm, without negative consequences for testing sensitivity fluctuations. The reduced fluctuations of CL of the order of 8 dB are rather high and still can cause problems during rail inspections.

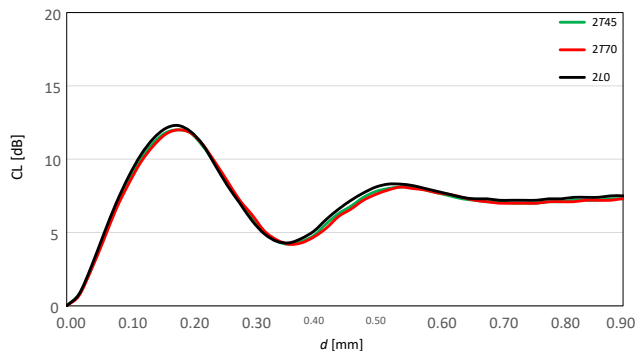


Fig. 7. Dependences of coupling losses on the coupling layer thickness for 2 MHz *L*-type probe and *T*-type probes with the same bandwidth (WB = 50%) but with different refraction angles; 2*T*45 – probe with transversal wave and refraction angle $\theta_3 = 45^\circ$; 2*T*70 – probe with transversal wave and refraction angle $\theta_3 = 70^\circ$; 2*L*0 – probe with longitudinal wave and refraction angle $\theta_3 = 0^\circ$.

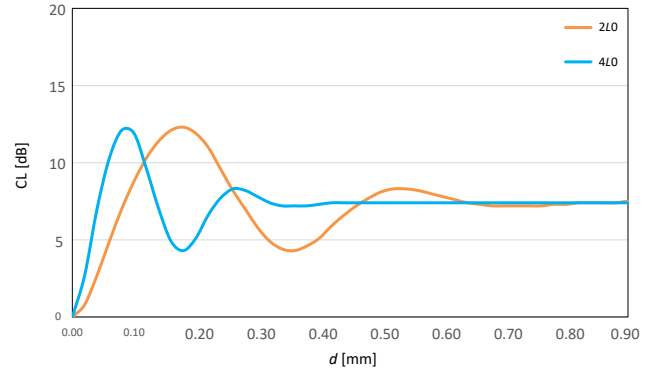


Fig. 8. Dependences of coupling losses on the coupling layer thickness for 2 MHz *L*-type probe and 4 MHz *L*-type probe with the same bandwidth (WB = 50%); 2*L*0 – 2 MHz probe with longitudinal wave and refraction angle $\theta_3 = 0^\circ$; 4*L*0 – 4 MHz probe with longitudinal wave and refraction angle $\theta_3 = 0^\circ$.

Using the presented model, one can search for other methods to reduce fluctuations of coupling losses. One of the possibilities is replacement of water with a coupling medium of higher acoustic impedance, e.g., glycerin. Unfortunately, this solution is impractical for a high speed ultrasonic inspection of railway rails due to environmental and technical constraints. Instead, one can investigate another solution consisting in replacing the conventional probe wedges made of PMMA with probe wedges made of Rexolite, that is a relatively new material which already entered ultrasonic applications. The Rexolite has lower acoustic impedance than PMMA (2.4 versus 3.2 Rayls) which is closer to water used as a coupling medium.

The coupling losses characteristic for 2 MHz probes with wedges made of PMMA and Rexolite are shown in Fig. 9. The maximum of the coupling losses for the Rexolite wedge is about 4.5 dB lower than the maximum for the PMMA wedge. After restriction of the minimal coupling layer to 0.10 mm, the amplitude of the testing sensitivity fluctuations will be reduced from 8 dB for PMMA wedges to 5 dB for Rexolite wedges.

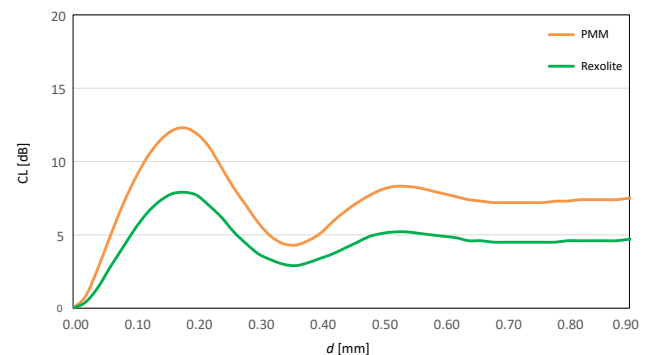


Fig. 9. Dependences of coupling losses on the coupling layer thickness for 2 MHz, WB = 50% probes with wedges made of PMMA and Rexolite.

The latter is a reasonably low value which may be compensated by scanning gain correction.

5. Conclusions

Losses determined for the case of beam transmission through the coupling layer between the ultrasonic probe emitting longitudinal or transverse waves and tested object, are presented in the article. As a standard, formulas for double transmission coefficients have so far been derived for harmonic waves of a strictly defined frequency. However, in practice, the pulses generated by modern ultrasonic probes used in non-destructive testing have a relatively wide frequency bandwidth. This means that the actual decrease in the amplitude of the ultrasonic pulse passing through the coupling layer from the probe to the tested material and vice versa is a certain average of the double transmission coefficients for all frequencies represented in the pulse spectrum. The numerical procedure presented in the paper takes into account the finite bandwidth of modern ultrasonic probes, which significantly changes the dependence of coupling losses on the thickness of the coupling layer. Contrary to the known analytical solutions, the model and program presented in the work allowed for precise calculation of coupling losses not only for normal beam probes producing longitudinal waves, but also for angle beam probes producing transversal waves, which are commonly used in non-destructive testing. Therefore, the developed model can be a significant improvement to the testing methodology for high speed ultrasonic inspection of railway rails, which can also be applied to other kinds of ultrasonic inspections, where fluctuation of the coupling layer thickness is an issue.

References

- BARNARD G.R., BARDIN J.L., WHITELEY J.W. (1975), Acoustic reflection and transmission characteristics for thin plates, *The Journal of the Acoustical Society of America*, **57**(3): 577–584, doi: 10.1121/1.380486.
- BRAY D.E. (2000), Historical review of technology development in NDE, [in:] *Proceedings of the 15th World Conference on NDT*, <https://www.ndt.net/search/docs.php3?id=1212> (access: 28.07.2023).
- BREKHOVSKIKH L.M. (1980), *Waves in Layered Media*, 2nd ed., Academic Press, New York.
- EN 16729-3 (2018), *Railway applications – Infrastructure – Non-destructive testing on rails in track – Part 3: Requirements for identifying internal and surface rail defects*, European Standards, <https://www.en-standard.eu/csn-en-16729-3-railway-applications-infrastructure-non-destructive-testing-on-rails-in-track-part-3-requirements-for-identifying-internal-and-surface-rail-defects/> (access: 28.07.2023).
- EN 17397-1 (2021), *Railway applications – Rail defects – Part 1: Rail defect management*, European Standards, <https://www.en-standard.eu/din-en-17397-1-railway-applications-rail-defects-part-1-rail-defect-management/> (access: 28.07.2023).
- EN ISO 22232-2 (2020), *Non-destructive testing – Characterization and verification of ultrasonic test equipment – Part 2: Probes*, European Standards, <https://standards.iteh.ai/catalog/standards/cen/c360d5ef-82bb-46cb-8868-c046f44b1c9d/en-iso-22232-2-2020> (access: 28.07.2023).
- Federal Railroad Administration (2015), *Track Inspector Rail Defect Reference Manual*, <https://railroads.dot.gov/elibrary/track-inspector-rail-defect-reference-manual> (access: 28.07.2023).
- FOLDS D.L., LOGGINS C.D. (1977), Transmission and reflection of ultrasonic waves in layered media, *The Journal of the Acoustical Society of America*, **62**(5): 1102–1109, doi: 10.1121/1.381643.
- HECKEL T., CASPERSON R., RUTHE S., MOOK G. (2018), Signal processing for non-destructive testing of railway tracks, [in:] *Proceedings of 44th Annual Review of Progress in Quantitative Nondestructive Evaluation*, **1949**(1): 030005, doi: 10.1063/1.5031528.
- HECKEL T., THOMAS H.M., KREUTZBRUCK M., RÜHE S. (2009), High speed non-destructive rail testing with advanced ultrasound and Eddy-current testing techniques, [in:] *Proceedings of the National Seminar & Exhibition on Non-Destructive Evaluation*, pp. 261–265.
- HECKEL T., WACK Y., MOOK G. (2019), Simulation of an instrumented ultrasonic test run with a rail inspection train, [in:] *Review of Progress in Quantitative Nondestructive Evaluation*, <https://www.iastatedigitalpress.com/qnde/article/id/8743/> (access: 28.11.2023).
- International Union of Railways [UIC] (2022), *UIC Safety Report 2022*, https://safetydb.uic.org/IMG/pdf/uic_safety_report_2022.pdf (access: 28.07.2023).
- KRAUTKRÄMER J., KRAUTKRÄMER H. (1990), *Ultrasonic Testing of Materials*, 4th ed., Springer Berlin, Heidelberg.
- OBRAZ J. (1983), *Ultrasound in Measurement Technique* [in Polish: *Ultradźwięki w Technice Pomiarowej*], Wydawnictwa Naukowo-Techniczne, Warszawa.
- PAPAEIAS M.P., ROBERTS C., DAVIS C.L. (2008), A review on non-destructive evaluation of rails: State-of-the-art and future development, *Proceedings of the Institution of Mechanical Engineers, Part F: Journal of Rail and Rapid Transit*, **222**(4): 367–384, doi: 10.1243/09544097JRR209.
- SCHMERR JR. L.W. (2016), *Fundamentals of Ultrasonic Nondestructive Evaluation. A Modelling Approach*, 2nd ed., Springer Cham.
- ZULIAN D. (2022), Effect of ultrasonic coupling media and surface roughness on contact transfer loss, *Coherent Engineering*, **9**(1): 2009092, doi: 10.1080/23311916.2021.2009092.